Title
Effects of Si/Al Ratio on the Distribution of Framework Al and on the Rates of Alkane Monomolecular Cracking and Dehydrogenation in H-MFI

Journal
Journal of the American Chemical Society, 135(51)

ISSN
0002-7863

Authors
Janda, Amber
Bell, Alexis T

Publication Date
2013-12-26

DOI
10.1021/ja4081937

Peer reviewed

JACS
JOURNAL OF THE AMERICAN CHEMICAL SOCIETY
Article
pubs.acs.org/JACS

Effects of Si/Al Ratio on the Distribution of Framework Al and on the Rates of Alkane Monomolecular Cracking and Dehydrogenation in H-MFI

Amber Janda and Alexis T. Bell*

Department of Chemical and Biomolecular Engineering, University of California—Berkeley, Berkeley, California 94720, United States

Supporting Information

ABSTRACT: The aim of this study was to investigate the influence of Si/Al ratio on the locations of exchangeable cations in H-MFI and on the monomolecular cracking and dehydrogenation reactions of *n*-butane. On the basis of UV−visible spectroscopic analysis of Co(II) exchanged into MFI, it was inferred that the fraction of Co(II) (and, by extension, Brønsted protons) located at channel intersections relative to straight and sinusoidal channels increases with increasing Al content. Concurrently, turnover frequencies for all monomolecular reactions, and the selectivities to dehydrogenation versus cracking and to terminal cracking versus central cracking, generally increased. The changes in selectivity with Al content are consistent with the finding that the transition-state geometry for dehydrogenation is bulky and resembles a product state, and should therefore exhibit a stronger preference to occur at channel intersections relative to cracking. Increases in turnover frequencies are attributed partly to increases in intrinsic activation entropies that compensate for concurrent increases in intrinsic activation energies, most strongly for dehydrogenation and terminal cracking, resulting in increased selectivity to these reactions at higher Al content. This interpretation contrasts with the view that intrinsic activation barriers are constant. It is also observed that isobutene inhibits the rate of *n*-butane dehydrogenation. Theoretical calculations indicate that this effect originates from adsorption of isobutene at the channel intersections. Because cracking reaction rates are not affected by the presence of isobutene, this result suggests that the preference of dehydrogenation to occur at channel intersections is much stronger than the preference for cracking to occur at these locations.

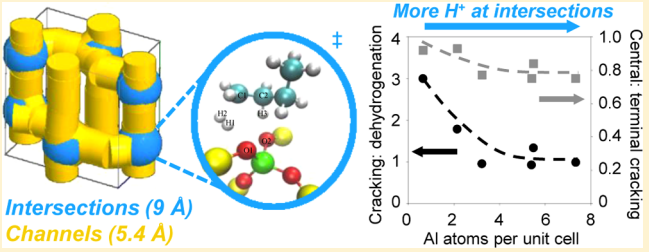

1. INTRODUCTION

Zeolites are used extensively in the petrochemical industry for the catalytic cracking of alkanes into lower molecular weight products. The channels and cavities that surround catalytically active Brønsted acid centers are similar in dimensions to reactant and product molecules and transition states, imparting shape-selective properties that facilitate the control of product distributions. At high temperatures and at sufficiently low conversions and partial pressures, alkanes react primarily via a monomolecular mechanism in which the alkanes interact directly with Brønsted protons.[1,2] These interactions lead to charged transition states that ultimately produce lower molecular weight alkanes, alkenes, and hydrogen. The intracrystalline diffusion of reactant molecules does not limit reaction rates for small alkanes and zeolite crystallites of typical dimensions (0.1−1.0 μm),[3−5] allowing experimental activation barriers to be compared directly to values predicted from theory.

Although the specific locations of Brønsted protons and framework Al atoms cannot be easily characterized for most zeolites, FTIR spectroscopy, UV−visible spectroscopy of Co(II)-exchanged zeolites, and ^{27}Al MAS NMR techniques, together with theoretical work, have provided strong evidence that the Al and proton distributions in MFI and other frameworks are nonrandom and depend on the Si/Al ratio and on synthesis parameters.[6−20] This raises the issue of whether changes in the distribution of Al among nonequivalent sites within a zeolite framework resulting from changes in the Si/Al ratio can affect the turnover frequencies for cracking and dehydrogenation. Differing answers to this question can be inferred from the literature. For example, Haag and Dessau have synthesized H-MFI samples spanning 3 orders of magnitude in Al concentration and have reported that the activity per tetrahedral Al for *n*-hexane monomolecular conversion is similar over the compositional range. This observation is consistent with either an invariant proton distribution or the insensitivity of *n*-hexane cracking to proton location within the samples studied.[21−23] By contrast, Gounder and Iglesia[24] have reported that turnover frequencies of propane cracking and dehydrogenation differed by up to a factor of 5 on H-MFI samples with different Si/Al ratios, but no systematic trends were discernible over the narrow range of Al content investigated. And for (H,Na)-MOR, Gounder and

Received: August 13, 2013
Published: November 15, 2013

dx.doi.org/10.1021/ja4081937 | J. Am. Chem. Soc. 2013, 135, 19193−19207

Iglesia[24] have observed that cracking and dehydrogenation of propane and *n*-butane occur at higher rates in the 8-MR side pockets than in the 12-MR channels. The authors conclude that transition states are contained only partially in the shallow 8-MR pores, resulting in greater apparent activation entropies and lower Gibbs free energies relative to those in the channels. These observations suggest that the original observation by Haag and co-workers of similar activity per tetrahedral Al cannot be generalized to other alkanes and zeolites or to MFI of different synthetic origin. Moreover, it appears that monomolecular reactions of propane and *n*-butane are reliable indicators of variances in proton locations among zeolites of the same structure, and that a study of the behavior of these reactions over a sufficiently wide range in Al content should provide insight into the specifics of the trends in Al and proton locations.[6−20] MFI is a good candidate for such a study because it can be synthesized readily over a wide range of Al concentration ($10 < Si/Al < \infty$) and the strengths of the acid sites over this range are constant, based on small variations in the measured heats of adsorption for ammonia[25,26] and on similar strengths of interaction of H_2 with zeolitic protons at low temperature.[27] Moreover, computational studies have shown that O−H bond enthalpies differ by no more than 11 kJ mol^{-1} among Brønsted acid sites associated with Al at each of the 12 crystallographic T-sites.[28,29]

We present evidence here that supports the existence of systematic trends in Brønsted proton location as a function of Al content in H-MFI samples obtained from a single source. Differences in the measured reaction rates, selectivities, and activation parameters observed with changes in Si/Al ratio are consistent with concurrent changes in the distribution of protons and the consequences of these changes on the confinement of transition states for elementary processes involved in *n*-butane cracking and dehydrogenation. Evidence for changes in the locations of active sites with Al concentration was deduced from an analysis of UV−visible spectra of Co(II)-exchanged MFI using the procedures described by Wichterlová, Dědeček, and co-workers.[7−11] Our work suggests that reactions of *n*-butane via monomolecular activation in H-MFI occur preferentially at Brønsted acid sites located in the channel intersections. We propose that this preference originates from the lower confinement of transition states at the intersections relative to the channels, leading to larger apparent and intrinsic activation entropies that offset correspondingly larger apparent and intrinsic activation enthalpies. Notably, this finding contrasts with the view that the intrinsic activation energy is constant for a given bond cleavage reaction, and that differences in activation energies are reducible to differences in the gas phase proton affinities of alkanes protonated at various C−C or C−H bonds.[24,30] Dehydrogenation appears to exhibit the strongest preference to occur at the intersections because the transition state for this reaction is the loosest and most strongly resembles a product state. Positive calculated values of the intrinsic activation entropy for dehydrogenation are consistent with this conclusion and can be rationalized using statistical mechanics. The preference for reaction at the intersections is least apparent for central cracking, which proceeds via an earlier and more constrained transition state. Unexpectedly, isobutene is found to have an inhibitory effect on the rates of *n*-butane dehydrogenation and secondary hydride transfer. Analysis of the thermodynamics of isobutene adsorption on Brønsted acid protons shows that the inhibition most likely results from adsorption at channel intersections and lends further support to the conclusion that *n*-butane dehydrogenation exhibits a very strong preference to occur at these locations within MFI.

2. METHODS

2.1. Catalyst Preparation and Textural Characterization. MFI zeolites with nominal Si/Al ratios of 140, 40, 25, 15, and 11.5 (Table 1) were obtained from Zeolyst International in the NH_4^+ form.

Table 1. Product Numbers, Si/Al Ratios, and Na/Al Ratios of H-MFI and Na-MFI Zeolites

		Si/Al ratio[a]		Na/Al ratio[a]
zeolite	product no.	H-MFI	Na-MFI	Na-MFI
MFI-140	CBV-28014	142 ± 48	137 ± 31	0.88 ± 0.25
MFI-40	CBV-8014	43.7 ± 6.5	44.8 ± 4.1	0.99 ± 0.08
MFI-25	CBV-5524G	28.8 ± 4.4	29.1 ± 4.0	0.90 ± 0.06
MFI-15(P)	CBV-3024E	16.5 ± 2.6	16.4 ± 2.5	0.84 ± 0.04
MFI-15(M)	CBV-3024E	16.7 ± 2.5	18.5 ± 2.1	0.84 ± 0.05
MFI-11.5	CBV-2314	12.1 ± 1.7	12.5 ± 1.8	0.99 ± 0.03

[a]Measured by Galbraith Laboratories using ICP-OES. Uncertainties are taken as twice the standard error calculated by propagation of the estimated uncertainties in Na, Si, and Al contents for a 50 mg sample (Al, ±0.03%; Na, ±0.03%; Si, ±2%).

Samples (~2 g) were placed in a quartz boat inside a quartz tube and heated at 2 K min^{-1} to 773 K in synthetic air (100 cm^3 min^{-1}, zero grade, Praxair). The zeolites were maintained at 773 K for 4 h to convert from the NH_4^+ to the H^+ form. A portion of H-MFI-15 was treated with ethylenediaminetetraacetic (EDTA) (see section 2.5) in an attempt to remove extraframework Al (EFAl). The parent and treated forms of this zeolite are denoted MFI-15(P) and MFI-15(M), respectively. Samples of H-MFI (~100−115 mg) were placed in test tubes and evacuated (<50 mTorr) at 393 K overnight before measurement of N_2 adsorption isotherms, which were measured at 77 K using a Micromeritics Gemini VII apparatus. Micropore volumes were calculated using the t-plot method of Lippens and de Boer and the Harkins−Jura equation for nonporous Al_2O_3 to model the statistical thickness.[31,32] To estimate the amount of framework Al associated with exchangeable Brønsted protons, the Na^+ form of each zeolite was prepared by treating 1−2 g of the H^+ form with 100 cm^3 of 1 M aqueous $NaNO_3$ at 353 K with magnetic stirring. After 6 h the mixture was vacuum-filtered and washed with deionized water. This procedure was repeated twice for a total of three treatments. The dry filtrate was then placed in the quartz boat and tube apparatus described above and heated to 393 at 1 K min^{-1} in synthetic air (100 cm^3 min^{-1}, zero grade, Praxair), held for 2 h, heated at 2 K min^{-1} to 773 K, and held for 4 h before cooling at 2 K min^{-1} to ambient temperature. (Co,Na)-MFI samples were prepared from each of the Na-MFI zeolites using a procedure that has been shown to produce (Co,Na)-MFI exchanged to the maximum degree and devoid of free and bridging cobalt oxides.[7,10] Zeolites (1−2 g) in the Na^+ form were added to 0.05 M $Co(NO_3)_2$ (50 cm^3 g^{-1}) prepared from $Co(NO_3)_2 \cdot 6(H_2O)$ (99%, Aldrich). The mixtures were stirred for 24 h in round-bottom flasks at room temperature and were then isolated by vacuum filtration. This procedure was performed three times for each sample. After the third treatment, the samples were washed with deionized water and filtered three times. Portions of filtrate were placed in test tubes under vacuum (<50 mTorr) and held overnight at 393 K before measurement of UV−visible spectra.

2.2. Quantification of Si, Al, and Brønsted Proton Contents. Total Si and Al contents were determined for all zeolites, and Na and Co contents were measured for Na-MFI and (Co,Na)-MFI zeolites, by Galbraith Laboratories using inductively coupled plasma optical emission spectroscopy (ICP-OES). The Na/Al ratios (Table 1) were ~1 within experimental uncertainty for all zeolites except for MFI-15(P) and MFI-15(M), which exhibited Na/Al ratios of 0.84. This result was assumed to indicate the presence of Al in nonexchangeable

extraframework positions. Maximum exchange by Na^+ was verified on the basis of the absence of a Brønsted O−H stretching peak observable at 3610 cm^{-1} in the infrared spectrum. Brønsted proton concentrations were measured by quantifying the decomposition products of dimethyl ether (DME) using online mass spectrometry.[33−35] The titrations were performed using a stainless steel reactor (1.27 cm outer diameter) pinched in the middle to hold a quartz wool support. H-MFI samples (0.180−0.344 g) were placed on top of the quartz wool and a K-type thermocouple was inserted directly into the catalyst bed. Samples were heated at 5 K min^{-1} in an electric furnace in synthetic air (100 cm^3 min^{-1}, zero grade, Praxair) using Omega controllers, held for 2 h at 773 K, and cooled to 438 at 5 K min^{-1}. DME (99.5%, Matheson) was then fed in pulses through a 0.65 cm^3 sample loop into a helium stream (160 cm^3 min^{-1}, 99.999%, Praxair) flowing over the catalyst. A mass spectrometer (MKS Spectra Minilab) was used to monitor the concentrations of DME (m/z 45, 46), water (m/z 18), and methanol (m/z 31, 32) for 4−8 h after introduction of the first pulse. The amount of DME introduced was determined by calibrating the pulses in a separate bypass loop. The quantity of DME consumed was calculated on the basis of the difference between the amount injected and the amount detected in the effluent after breakthrough. Only H_2O was detected above baseline levels; thus, the number of Brønsted protons titrated was assumed to be equal to twice the number of DME molecules reacted.

2.3. Assessment of Relative Numbers of Brønsted and Lewis Acid Centers. The relative concentrations of Brønsted and Lewis acid sites were inferred from infrared spectra of adsorbed pyridine at 473 K. Spectra were collected using a Nicolet 6700 FTIR spectrometer (Thermo Scientific) equipped with a Hg-Cd-Te (MCT) detector cooled by liquid nitrogen. Self-supporting zeolite wafers (40−75 mg) were suspended between CaF_2 windows in a cylindrical cell similar to that described in ref 36. The sample was then heated to 773 K at 5 K min^{-1} in synthetic air (100 cm^3 min^{-1}, zero grade, Praxair), held for 2 h, and cooled to 473 K at 5 K min^{-1} prior to adsorption experiments. Pyridine (99.8%, Aldrich) was injected into the cell via a septum until IR peak intensities remained constant. The cell was left in flowing He for 1−2 h to allow physisorbed pyridine to desorb. Spectra were then recorded and averaged over 32−128 scans between 1250 and 4000 cm^{-1} with 0.5 cm^{-1} resolution. Peak areas corresponding to pyridine adsorbed at Brønsted (1545 cm^{-1}) and Lewis (1450 cm^{-1}) acid sites[37] were normalized to the areas of framework combination and overtone bands appearing between 1750 and 2100 cm^{-1} and then divided by their respective extinction coefficients,[38] 0.73 and 0.96 cm μmol^{-1}. Infrared spectra of H-MFI without adsorbate were collected by following the above procedure, but cooling instead to ambient temperature in flowing He after calcination at 773 K.

2.4. Assessment of the Distribution and Concentration of Co(II). UV−visible spectra were measured using an Evolution 300 UV−visible spectrophotometer (Thermo Scientific) equipped with an in situ flow cell (Harrick) and a Praying Mantis diffuse reflectance accessory (Harrick). Spectra were collected between 200 and 700 nm with 2 nm resolution. (Co,Na)-MFI samples were heated using Watlow 988 controllers to 713 at 5 K min^{-1} in flowing He (100 cm^3 min^{-1}, 99.999%, Praxair), held for 3−4 h to drive off adsorbed water, and then cooled to 393 K for the collection of spectra. Absorption intensities were extracted from reflectance data using the Schuster−Kubelka−Munck equation. After baseline correction the spectra were deconvoluted into Gaussian bands using the peak positions reported previously.[7,10,39] The measured peak areas and published absorption coefficients were used to assess the relative concentrations of Co(II) at α (straight channel), γ (sinusoidal channel), and β (intersection) positions. A detailed description of the locations of these sites within the MFI framework is provided in the Supporting Information.

2.5. Extraction of Extraframework Al. H-MFI-15(P) was treated with EDTA with the intent of removing EFAl material. The concern was that the EFAl could alter the acidity or environment of Brønsted protons and, consequently, their catalytic behavior.[33,38,40,41] Therefore, MFI-15(P) was subjected to a procedure similar to that of Gola et al.,[42] who reported a treatment in which EDTA was found to extract EFAl from FAU without also removing framework Al or decreasing the crystallinity. The parent H-MFI-15(P) (774 mg, 0.74 mmol total Al) and 0.45 g of EDTA (1.54 mmol) were added to 50 cm^3 of deionized water, heated to 348 K with magnetic stirring for 2 h, filtered over vacuum, and rinsed. The filtrate was then added to 50 cm^3 of 1 M NH_4NO_3, stirred at 363 K for 6 h, filtered, and washed. The sample was then placed in a quartz boat and tube apparatus, heated at 1 K min^{-1} in flowing air to 393 K, and held for 2 h. The temperature was then increased at 1 K min^{-1} to 853 K and held for 6 h to burn off residual organics. A portion of the calcined sample (MFI-15(M) in Table 1) was exchanged three times in 1 M aqueous $NaNO_3$ as described in section 2.1 to produce Na-MFI-15(M). Samples of H-MFI-15(P) and EDTA-modified H-MFI-15(M) were characterized by X-ray diffraction (XRD) to assess any changes in the crystallinity caused by the treatment. Samples were immobilized on flat plates with petroleum jelly and analyzed using a Siemens D-5000 diffractometer with Cu Kα radiation and a scintillation counter detector. Data were recorded digitally at 2θ of 7−35° with a step size of 0.015°. Diffractograms appeared similar and were consistent with a crystalline MFI structure.

2.6. Catalytic Rate Measurements. A tubular quartz reactor (6.5 mm outer diameter) was used for measurements of reaction rates. These data were acquired using 8−15 mg of catalyst, with the exception of MFI-140. A similar quartz reactor with a cylindrical bubble (12.7 mm outer diameter) was used for MFI-140 samples (70−80 mg) because of their low concentration of active sites. In both reactors, catalyst beds were supported on fresh quartz wool held in place at a pinch. The reactor was heated by a three-zone furnace with K-type thermocouples in each zone controlled by Watlow 988 controllers. An additional thermocouple was placed at the reactor wall next to the catalyst bed to verify that the temperature reading matched that of controlled zones. Pressure measurements were read from gauges placed at the inlet and exit of the reactor just outside of the furnace. Pressure drops across the reactor were small (<5%) for conditions used in this work. Catalyst samples were heated at 5 K min^{-1} to 773 K in flowing 10% O_2 in He (30−100 cm^3 min^{-1}, Praxair) and held for 2 h prior to initiating reactions at 773 K. Helium (99.999%, Praxair) was then passed over the catalyst while the feed flow rates of *n*-butane and helium were adjusted in a bypass loop. Feed and effluent streams were sent through heated tubing to a Varian CP-3800 gas chromatograph, separated by a Varian CP-Al_2O_3/Na_2SO_4 capillary column (5 μm, 0.32 mm i.d. × 50 m) and analyzed by flame ionization detection. The amount of H_2 in the products was too low to be quantified by thermal conductivity detection and was, therefore, estimated by performing a steady-state atom balance on C and H. The H:C ratio in the products was constrained to a value of 10:4 for butane (C_4H_{10}), allowing the quantity of H_2 formed to be calculated.

Rate measurements were performed after an initial transient period during which the cracking rates remained nearly constant but dehydrogenation rates decayed with time on stream except for MFI-11.5, which, unexpectedly, activated with increasing time on stream. We suggest that a Lewis acid site is responsible for the initial dehydrogenation activity[43] on MFI-140, MFI-40, MFI-25, and MFI-15 because the rates of cracking and the small but detectable rates of secondary hydride transfer—reactions that are catalyzed by Brønsted acid sites—do not deactivate concurrently (see Supporting Information). Other researchers have performed analyses of the relative rates of intracrystalline and intraparticle diffusion of reactant and of monomolecular activation reactions for butanes and propane on MFI, MOR, and MWW.[24,34] These authors conclude that the reaction rates measured for these systems are not influenced by rates of mass transport, a conclusion that can be extended to MFI zeolites and *n*-butane.

Rate measurements were performed under differential conditions (conversion <1.5%) between 723 and 788 K. The rate of each monomolecular reaction was calculated on the basis of the rate of appearance of the alkane (or H_2) product because these products undergo virtually no secondary conversion under the conditions of our experiments. The selectivity to each reaction was defined as the ratio of the rate of formation of the alkane (or H_2) product divided by the total rate of formation of these products. First-order rate coefficients

were measured at fixed space times by varying the flow rate of *n*-butane (99.9%, Matheson) in He (99.999%, Praxair) at constant total flow rate. The rate coefficients so obtained were then extrapolated to zero space time (see Supporting Information) in order to obtain values corresponding to conditions of zero conversion. Product pair ratios (C_2H_6:C_2H_4, CH_4:C_3H_6, H_2:C_4H_8) varied only weakly with space time and extrapolated to ~1 at zero space time. Products containing more than four carbon atoms were not observed, but small amounts of propane and isobutane (<3% of products) were produced by hydride transfer from *n*-butane to propene and isobutene, respectively. The rates of formation of these products approached zero in the limit of zero conversion.

The effects of butene and propene concentrations on rates and selectivities were probed by co-feeding isobutene (99%, Aldrich) or propene (99%, Aldrich) with *n*-butane during the rate measurements. A stream of ~0.25% alkene was created by dilution in He (220 cm^3 min^{-1}, 99.999%, Praxair). A small portion of this stream (<3 cm^3 min^{-1}) was introduced via a mass flow controller to the butane and He feed in order to achieve propene and butene partial pressures representative of conditions of the rate measurements (~10^{-4} atm).

3. RESULTS AND DISCUSSION

3.1. Catalyst Characterization. The results of zeolite characterization are presented in Tables 1−4. Micropore volumes calculated using the t-plot method are given in Table 2. Zeolites with nominal Si/Al ratios of 40 and greater

Table 2. Nitrogen Micropore Volumes of MFI Zeolites and Infrared Spectroscopic Analyses of Adsorbed Pyridine

	infrared peak areas[a]			
zeolite	Py-H^+	Py-L	Py-H^+/Py-L ratio	micropore volume (cm^3 g^{-1})
MFI-140	0.006	0.001	6.2	0.131
MFI-40	0.033	0.004	8.0	0.130
MFI-25	0.054	0.005	10.5	0.132
MFI-15(P)	0.092	0.011	8.6	0.131
MFI-15(M)	0.090	0.009	9.8	0.129
MFI-11.5	0.180	0.011	16.7	0.138

[a]Integrated peak areas for pyridine adsorbed at Brønsted (Py-H^+) and Lewis (Py-L) acid sites are normalized to areas corresponding to framework vibrations (1750−2100 cm^{-1}) and divided by extinction coefficients taken from ref 38.

exhibited typical type I nitrogen isotherms (not shown), while the isotherm for MFI-140 had two plateaus; a lower plateau below a relative pressure of ~0.15 and a second one above a relative pressure ~0.2. This behavior is well documented for MFI with low Al content (Si/Al ratio >45) and has been linked to the reordering of adsorbed nitrogen from a fluid-like to solid-like state.[44−50] The micropore volume reported for MFI-140 was calculated using data from the second plateau of the isotherm. There is no trend in micropore volume with respect to Si/Al ratio and the micropore volumes in Table 2 are similar to the values reported previously for MFI (~0.13 cm^3 g^{-1}).[44−46]

The Si/Al ratios of the H^+ and Na^+ forms of each zeolite are given in Table 1 and are similar within experimental error, indicating that any cationic EFAl[38,51−53] that may have been present in the H-MFI zeolites did not exchange to a significant extent with Na^+ and that the Na/Al ratio is a reliable proxy for the fraction of Al associated with a proton. The Na/Al ratios (Table 1) were near unity within the estimated experimental uncertainties except for the values of 0.84 obtained for MFI-15(P) and MFI-15(M). Also, with the exception of MFI-15(P) and MFI-15(M), which had H^+/Al ratios of ~0.8 (Table 3), the proton counts measured by DME titration are very similar to

Table 3. Total Al (Al_{tot}) and Brønsted Proton (H^+) Counts Per Unit Cell, and H^+/Al_{tot} Ratios for MFI Zeolites

zeolite	H^+/unit cell	Al_{tot}/unit cell[a]	H^+/Al_{tot} ratio
MFI-140	0.62	0.67	0.93
MFI-40	1.94	2.15	0.91
MFI-25	3.19	3.23	0.99
MFI-15(P)	4.33	5.49	0.80
MFI-15(M)	4.35	5.41	0.79
MFI-11.5	7.24	7.34	0.99

[a]Calculated using Si/Al ratios of H-MFI, taken from Table 1, and the MFI unit cell formula: Al/u.c. = 96/(1+Si/Al).

the total Al contents determined by ICP-OES. These results demonstrate that EFAl is present in low quantities relative to framework Al in MFI-140, MFI-40, MFI-25, and in MFI-11.5, but comprises 15−20% of the Al in MFI-15(P) and in MFI-15(M). Therefore, at best a partial extraction of EFAl was achieved by treatment of MFI-15(P) with EDTA. However, because of the similarities in the Na/Al and H^+/Al ratios of these two samples, it is difficult to assess the fraction of EDTA removed. Further analyses of MFI-15(M) and MFI-15(P) (see Supporting Information) indicate that the EFAl is at least partly non-hydroxylated and that a redispersion, transformation, or migration of the material has occurred during EDTA treatment; such behavior has been suggested on the basis of previous spectroscopic studies.[38,51,54,57,58] The ratios of Brønsted to Lewis acid sites, included in Table 2, increase from a value of ~6 for MFI-140 to a value of ~17 for MFI-11.5. The increase in this ratio is not surprising since the concentration of EFAl—associated with Lewis acidity[40,54−56]—does not increase with the Al content.

Elemental analyses of (Co,Na)-MFI zeolites and the distribution of Co(II) among the channels and intersections of the zeolites are presented in Table 4. Values of the ratio (2Co + Na)/Al are expected to equal unity to satisfy charge neutrality. These values are less than unity for our samples, despite Na/Al ratios that were close to 1 (Table 1) for the Na-MFI samples that were treated with $Co(NO_3)_2$. This result indicates that some exchange of Na^+ with H^+ occurred during the treatment, which has been reported previously.[10,59,60] The lower values of this ratio for our samples compared to previous work, in which the ratio did not fall below 0.87, are likely a consequence of the longer time that we allowed for the exchange process. The experimental spectra (numerically smoothed and normalized to the largest spectral intensities) and an example of a deconvoluted spectrum are presented in Figure 1a and b, respectively. The relative areas of the four components of the β feature are the same as those reported by Dědeček et al.[7] for a number of zeolites, and a good fit of the experimental spectrum is obtained for all samples. The fraction of Co(II) located at straight channels (α), sinusoidal channels (γ), and intersections (β), the ratio of Co(II) in the channels to Co(II) in the intersections, and the ratio of Co(II) in the sinusoidal channels to that in the straight channels are plotted versus the Al concentration in Figure 2a and b, respectively. The percentage of cobalt occupying the channel intersections increases with the Al content up to 5.4 Al per unit cell (corresponding to MFI-15) and remains similar at the highest Al concentration. Concurrent with the overall increase in the

dx.doi.org/10.1021/ja4081937 | J. Am. Chem. Soc. 2013, 135, 19193−19207

Table 4. Ratios of Co, Na, and Al Contents, and Distribution of Co(II) in MFI Zeolites

			Co(II) distribution[b]				
zeolite	(2Co + Na)/Al[a]	$2Co/Al_{tot}$[a]	α	β	γ	$(\alpha+\gamma)/\beta$	γ/α
MFI-140	0.178	0.059	n.m.[c]	n.m.[c]	n.m.[c]	n.m.[c]	n.m.[c]
MFI-40	0.627	0.322	0.38	0.58	0.04	0.72	0.11
MFI-25	0.594	0.356	0.33	0.63	0.04	0.58	0.12
MFI-15(P)	0.644	0.394	0.24	0.71	0.05	0.41	0.23
MFI-11.5	0.871	0.556	0.23	0.69	0.08	0.44	0.34

[a]Measured by Galbraith Laboratories using ICP-OES. [b]Estimated by using spectral deconvolution methods reported elsewhere.[7,10,39] [c]Not measured because of low cobalt concentration and low UV−visible spectral intensities.

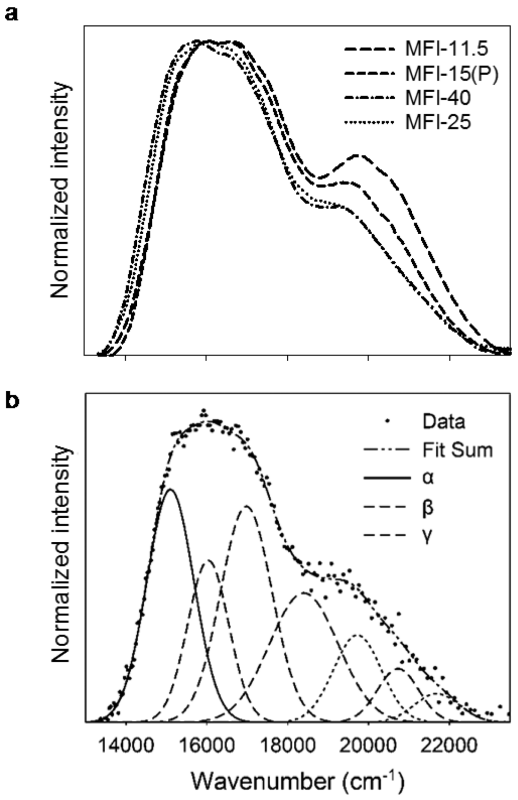

Figure 1. a) Experimental spectra for all (Co,Na)-MFI samples, numerically smoothed for ease of visualization. (b) Normalized UV−visible spectrum of (Co,Na)-MFI-25. Experimental data are shown as points. Spectral components and the fitted sum of the components are indicated with lines.

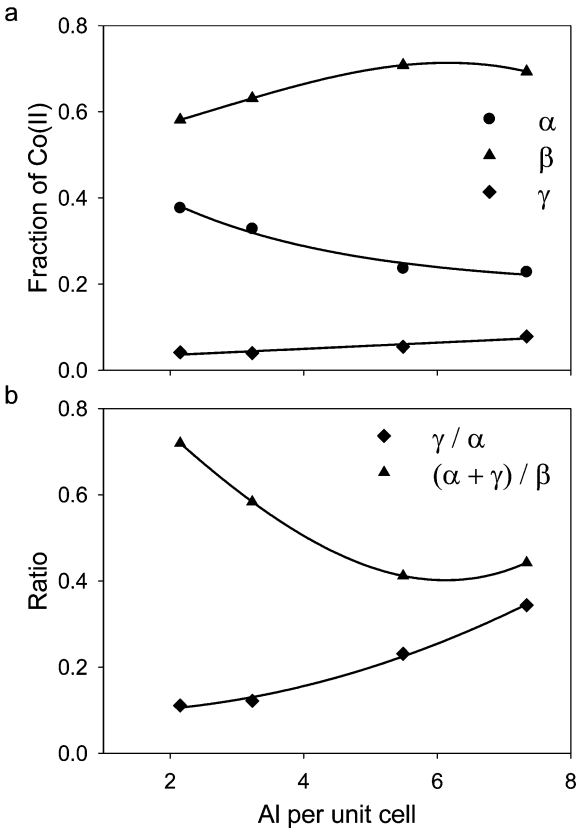

Figure 2. (a) Plot of the distribution of Co(II) among straight and sinusoidal channels and intersections. (b) Plot of the ratio of Co(II) in channels versus intersections and ratio of Co(II) in sinusoidal channels relative to straight channels.

fraction of Co(II) at the intersections, the distribution of Co(II) located in the channels shifts monotonically toward a greater fraction in the sinusoidal channels. These trends resemble those reported in ref 10 for sample set B. The observed trends in Co(II) siting show that Al-(O-Si-)$_2$-Al sequences within 6-MR[19] vary in a systematic fashion with Al concentration. While this does not demonstrate conclusively that similar variations exist in the locations of protons, a statistical analysis of Al distributions in MFI reported by Rice et al.[61] shows that the distributions of single Al atoms and next-nearest-neighbor Al atoms (Al-O-Si-O-Al sequences) in MFI are qualitatively similar. By extension, this suggests that trends in the distribution of Al-(O-Si-)$_2$-Al sequences, determined from analysis of UV−visible spectra of Co(II), approximate trends in the distribution of more isolated Al atoms. Even if this is not the case, the conclusions reached in this work require only that the *overall* distribution of Al varies in a similar way to that shown in Figure 2 for Co(II). Even if isolated Al atoms are distributed randomly, or their distribution is weakly to moderately anti-correlated with that of paired Al, the overall distribution of Al should still change in a direction that is consistent with Figure 2.

3.2. Kinetics and Elementary Steps of Monomolecular Alkane Activation Reactions. Prior to discussing the effects of Al concentration on the specific activity of H-MFI for *n*-butane cracking and dehydrogenation, it is useful to outline the mechanism by which these reactions occur and the reaction kinetics derived from this mechanism. The elementary steps involved in monomolecular reactions of alkanes are described by eqs 1 and 2, and the relative enthalpies of reactants, transition states, and products are illustrated in Figure 3. Alkane molecules in the gas phase, A(g), are physisorbed into the zeolite pores and are stabilized enthalpically by the heat of physisorption, ΔH_{phys}. The physisorbed state, A(z), and the

dx.doi.org/10.1021/ja4081937 | J. Am. Chem. Soc. 2013, 135, 19193−19207

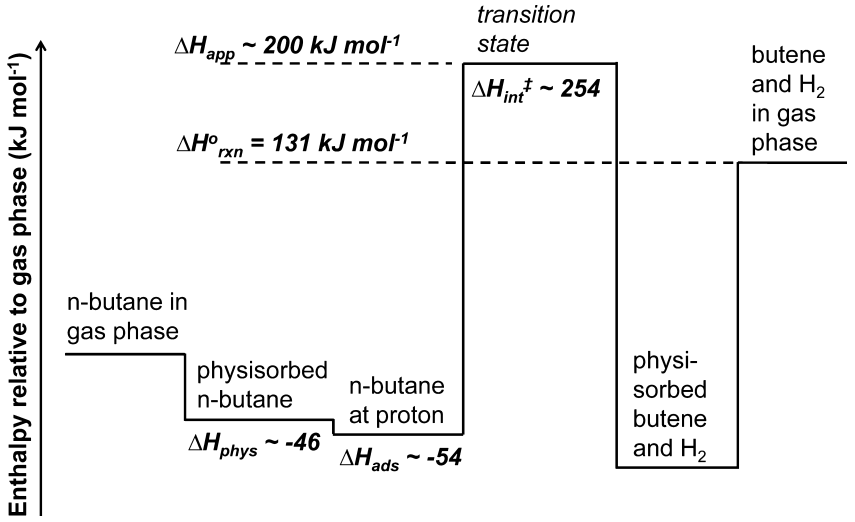

Figure 3. Illustration of the enthalpy changes involved in the elementary steps of monomolecular reactions of alkanes over acidic zeolites. Enthalpy values are indicated in the diagram for the dehydrogenation of n-butane. The standard enthalpy of reaction ΔH°_{rxn} has been extrapolated to 773 K from standard enthalpies of formation of *n*-butane, hydrogen and 1-butene at 1 bar and 298 K taken from ref 62.

enthalpy of physisorption, ΔH_{phys}, represent ensemble averages over all possible configurations of the alkane. In some configurations, the alkane is close enough to a Brønsted proton (Z−OH) to initiate cracking or dehydrogenation. These configurations are referred to collectively as the reactant state, A(r).

$$A(g) \rightleftarrows A(z) \rightleftarrows A(r) \tag{1}$$

$$A(r) + Z{-}OH \rightleftarrows [TS]^{\ddagger} \rightarrow \text{products}(z) + Z{-}OH \tag{2}$$

Swisher et al.[63] define the reactant state as those configurations in which an alkane C−C bond is within 5 Å of an Al T-atom. There is a small decrease in enthalpy (~7−10 kJ mol^{-1} for MFI)[64,65] between the physisorbed and localized states due to the specific interaction of the alkane with a proton, as shown in Figure 3. The gaseous, physisorbed, and reactant state alkanes are presumed to be in quasi-equilibrium according to eq 1. In the rate-determining step (eq 2), a Brønsted proton attacks an alkane molecule to produce a transition-state structure that is in quasi-equilibrium with the reactant state. The measured rate of reaction per active site, i.e., the turnover frequency (TOF), is proportional to the concentration of reactant state, $C_{A(r)}$, and the intrinsic rate coefficient, k_{int}, according to

$$\text{TOF} = k_{int}\frac{C_{A(r)}}{C_{H^+}} \tag{3}$$

where C_{H^+} is the concentration of protons in mol (kg zeolite)$^{-1}$. The intrinsic rate coefficient is given by absolute rate theory as

$$k_{int} = \frac{k_B T}{h}\exp\left(-\frac{\Delta G^{\ddagger}_{int}}{RT}\right) \tag{4}$$

where $\Delta G^{\ddagger}_{int}$ is the Gibbs free energy of activation. At the high temperatures and low partial pressures used for the experiments in this work, the concentration of *n*-butane at Brønsted protons is very low (see Supporting Information). Under such conditions the concentration of physisorbed alkane, $C_{A(z)}$, is proportional to the gas-phase partial pressure $P_{A(g)}$ and the Henry coefficient, K_H. The reactant-state concentration in moles per unit mass of zeolite can then be written as

$$C_{A(r)} = P_r K_H P_{A(g)} \tag{5}$$

where P_r is the (dimensionless) probability that the physisorbed alkane is localized at a proton. The concentration of alkane per active site[63] (dimensionless) is obtained by dividing eq 5 by C_{H^+}:

$$\frac{C_{A(r)}}{C_{H^+}} = p_r K_H P_{A(g)} \tag{6}$$

The probability P_r in eq 5 is proportional to C_{H^+}; thus, the value of p_r (lower case) in eq 6 is constant and has units of (kg zeolite) mol^{-1}. We define the Henry constant as

$$K_H = \frac{f_{pore}}{\rho_f RT}\exp\left(-\frac{\Delta G_{phys}}{RT}\right) \tag{7}$$

where f_{pore} is the fraction of the total volume that is accessible to the physisorbed alkane. The value of f_{pore} for a molecule of a specified characteristic dimension can be calculated according to computational methodology described by First et al.[66] or can be approximated as the product of an experimentally measured micropore volume and the mass density of the zeolite framework, ρ_f. We define the probability of an alkane molecule being in a reactant state (P_r) in terms of the Gibbs free energy change between the physisorbed and localized states (ΔG_r) as

$$P_r = f_{H^+}\exp\left(-\frac{\Delta G_r}{RT}\right) \tag{8}$$

where f_{H^+} is the fraction of the accessible pore volume that is contained within a 5 Å radius of an Al atom. The free energy change ΔG_r is a function of the type of reactant state complex being formed (e.g., central or terminal cracking) and the Al T-atom location (see Supporting Information). The fraction f_{H^+} can be written as the product of the proton concentration C_{H^+} and the volume contained in one mole of reactant state, V_{H^+} (m^3 mol^{-1}), divided by the accessible pore volume, V_{pore} (m^3 [kg zeolite]$^{-1}$):

dx.doi.org/10.1021/ja4081937 | J. Am. Chem. Soc. 2013, 135, 19193−19207

$$f_{H^+} = \frac{C_{H^+}V_{H^+}}{V_{pore}} \quad (9)$$

Combining eqs 3−9 gives an expression for the turnover frequency:

$$\mathrm{TOF} = \frac{\nu_{H^+}}{k_B T} K_{ads} k_{int} P_{A(g)} = \frac{\nu_{H^+}}{h} \exp\left(-\frac{\Delta G_{ads} + \Delta G^{\ddagger}_{int}}{RT}\right) P_{A(g)} \quad (10)$$

where K_{ads} is the dimensionless thermodynamic equilibrium constant for adsorption from the gas phase to a reactant state, and ΔG_{ads} is the corresponding change in the free energy. The value of ΔG_{ads} is equal to the sum of the free energy changes for physisorption and localization:

$$\Delta G_{ads} = \Delta G_{phys} + \Delta G_r \quad (11)$$

The volume of reactant state surrounding a single Al atom, ν_{H^+}, is equivalent to V_{H^+} divided by Avogadro's number. According to the definition given by Swisher et al.,[63] this volume is a sphere with radius extending 5 Å from the Al atom. The apparent first-order rate coefficient, based on the expression for the TOF (eq 10), is then given by

$$k_{app} = \frac{\nu_{H^+}}{h} \exp\left(-\frac{\Delta G_{ads} + \Delta G^{\ddagger}_{int}}{RT}\right) \quad (12)$$

and has units of mol (mol H^+)$^{-1}$ s^{-1} Pa^{-1}.

Using the relationship between the Gibbs free energy and the enthalpy and entropy ($\Delta G = \Delta H - T\Delta S$), the apparent entropy and energy of activation are obtained, respectively, from the intercept ($\ln k_{app,T\to\infty}$) and slope ($\partial \ln k_{app}/\partial[1/T]$) of an Arrhenius plot after normalizing k_{app} to the number of indistinguishable bonds for a given reaction pathway:

$$\Delta S_{app} = \Delta S_{ads} + \Delta S^{\ddagger}_{int} = R\left[\ln k_{app,T\to\infty} - \ln \frac{\nu_{H^+}}{h}\right] \quad (13)$$

$$E_{app} \approx \Delta H_{ads} + E^{\ddagger}_{int} = -R\left[\frac{\partial \ln k_{app}}{\partial(1/T)}\right] \quad (14)$$

It should be noted that the derivation given above does not require the specification of standard states for gaseous or adsorbed species. The choices of values for these standard states influence the magnitude and sign of the adsorption entropy[67−70] and the apparent activation entropy. Therefore, in comparing apparent activation entropies to literature values, reported data have been used to calculate the activation entropies according to equations presented in this section.

3.3. Influence of the Al Content on Apparent Rates, Selectivities, and Activation Parameters. Rate coefficients, selectivities, and ratios of selectivities measured at 773 K are given in Table 5 for *n*-butane cracking and dehydrogenation, and plots of these data versus the Al concentration (in Al atoms per unit cell) are presented in Figures 4 and 5, respectively. As seen in Figure 4, the rates of all three reactions increase with Al content up to 5.4 Al per unit cell (corresponding to MFI-15) and then decrease at the highest Al content of 7.3 Al per unit cell (corresponding to MFI-11.5). On the other hand, as shown in Figure 5, selectivities to dehydrogenation over cracking and to terminal cracking over central cracking increase nearly monotonically with the Al content when MFI-15(M) is chosen to represent the Al concentration of 5.4 Al per unit cell. The different catalytic behavior of MFI-15(M) compared to MFI-15(P) is hypothesized to be a consequence of the partial removal or disaggregation of EFAl within the pores and the consequent reduction of the influence of EFAl on the local environment of Brønsted acid sites in MFI-15(M) (see Supporting Information).

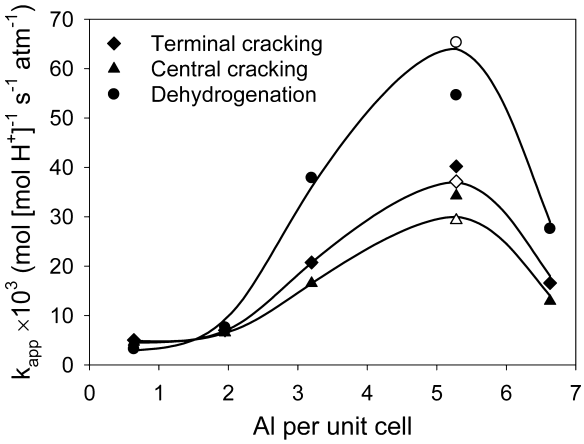

Figure 4. First-order rate coefficients of monomolecular cracking and dehydrogenation of *n*-butane versus Al atoms per unit cell in H-MFI. Data for MFI-15(M), which was treated with EDTA, are indicated with hollow symbols.

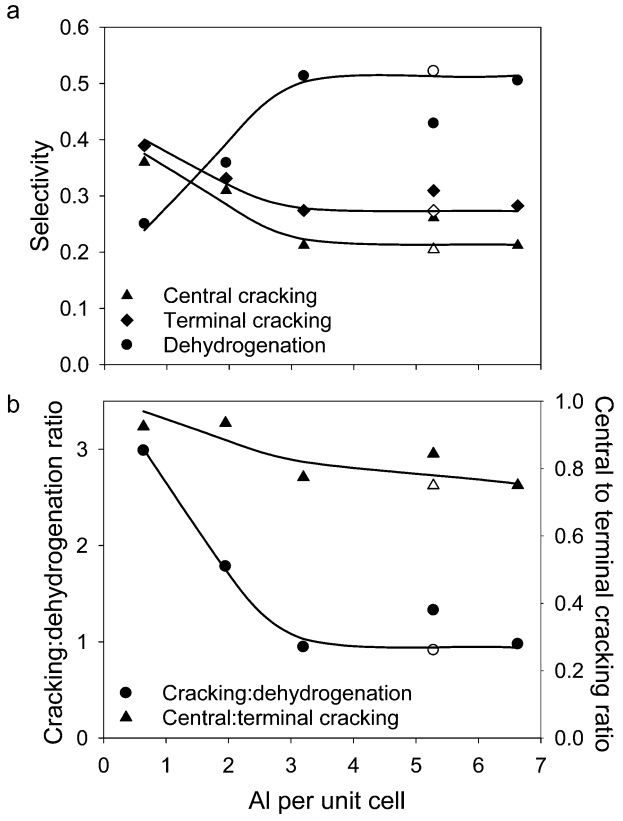

Figure 5. Selectivities (a) and selectivity ratios (b) for monomolecular *n*-butane reactions versus Al atoms per unit cell in H-MFI. Data for MFI-15(M), which was treated with EDTA, are indicated with hollow symbols.

Included in Table 5 are rate and selectivity data taken from the literature for MFI and for MOR.[24,71−74] In all work cited for MFI, the authors have indicated that the sample employed had a Si/Al ratio of 35 (2.67 Al per unit cell) and was obtained from

dx.doi.org/10.1021/ja4081937 | J. Am. Chem. Soc. 2013, 135, 19193−19207

Table 5. Rate Coefficients, Selectivities, and Selectivity Ratios of Monomolecular *n*-Butane Cracking and Dehydrogenation at 773 K

		k_{app} ($\times 10^3$ mol (mol H^+)$^{-1}$ s^{-1} atm^{-1})			selectivities			selectivity ratios	
zeolite	ref	central cracking	terminal cracking	dehydrogenation	central cracking	terminal cracking	dehydrogenation	central/terminal cracking	cracking/ dehydrogenation
MFI-140		4.7	5.0	3.2	0.36	0.39	0.25	0.92	2.99
MFI-40		6.5	7.0	7.6	0.31	0.33	0.36	0.93	1.78
MFI-25		16.5	20.7	37.9	0.21	0.27	0.51	0.77	0.95
MFI-15(P)		34.3	40.2	54.6	0.26	0.31	0.43	0.84	1.33
MFI-15(M)		29.3	37.1	65.3	0.20	0.27	0.52	0.75	0.92
MFI-11.5		12.9	16.6	27.6	0.21	0.28	0.51	0.75	0.98
MFI-35	71[a]	12.1	13.9	6.7	0.37	0.42	0.21	0.87	3.89
	72[b]	12.1	12.1	10.5	0.35	0.35	0.30	–	2.29
	73, 74	8.7	8.9	6.8	0.36	0.37	0.28	0.98	2.60
MOR 8-MR	24[c]	9.5	49.2	97.6	0.06	0.31	0.62	0.19	0.60
MOR 12-MR	24[c]	3.7	n.d.[d]	n.d.[d]	1.00	n.d.[d]	n.d.[d]	–	–

[a]Rate and selectivity data reported for 769 K have been extrapolated to 773 K using the authors' reported activation energies. [b]Cracking selectivities were estimated by dividing the reported overall selectivity to cracking by 2. [c]Rate and selectivity data reported for 748 K have been extrapolated to 773 K using the authors' reported activation energies. [d]Not detected.

Mobil. The rate coefficients for our H-MFI samples are similar in magnitude to those reported in the literature for H-MFI with similar Al content, but the selectivities to dehydrogenation reported in the literature are lower. The dissimilarities between our results and those of other researchers are not surprising given that the synthesis conditions were presumably different for the zeolites used in these studies, and it is known that the conditions of synthesis influence the siting of Al and Brønsted protons.[7−19] However, the reaction conditions under which the rate measurements were taken (see below) may also influence the measured rates. It can be seen in Table 5 that the rate coefficients for a given reaction pathway differ by up to a factor of 5−6. According to eq 6, the concentration of alkane per active site and, therefore, the rate coefficients, are proportional to the Henry constant (K_H) and the normalized probability that an alkane is in a reactant state (p_r). We believe that a difference of a factor of 6 among values of k_{app} in H-MFI is too large to be caused solely by changes in K_H and p_r that result from changes in the Si/Al ratio[75] or the Al distribution (see Supporting Information). Therefore, we conclude that changes in the intrinsic rate coefficients with Al content must influence the trends observed in k_{app}. As discussed below, these trends are proposed to be consequences of concurrent changes in the distribution of Al and Brønsted protons. Evidence for this proposal is suggested by the data presented in Figure 2, which shows that the fraction of Co(II) located within channel intersections (β-sites) rather than in the straight and sinusoidal channels (α- and γ-sites) increases with the content of Al in the zeolite framework. The question now is whether these changes are reflected in the rate and activation parameters for *n*-butane monomolecular cracking and dehydrogenation. To answer this question, it is useful to summarize what is known about the effects of proton location on these reactions in other zeolites, and whether similar effects might be anticipated for MFI.

Gounder and Iglesia have reported kinetic data for *n*-butane monomolecular cracking and dehydrogenation reactions at 8- and 12-MR locations in (H,Na)-MOR zeolites prepared from a single original sample.[24] These authors have found that the selectivities to dehydrogenation versus cracking and to terminal cracking versus central cracking at 748 K increase with the percentage of protons located at 8-MR sites. The effects of increasing the Al content in H-MFI on the selectivities of *n*-butane monomolecular cracking and dehydrogenation are, therefore, similar to the effects of increasing the fraction of protons in the 8-MR pockets of MOR. Gounder and Iglesia[24] have attributed these trends for MOR to the partial containment of transition states in the shallow 8-MR pores, resulting in greater entropies and lower Gibbs free energies of activation relative to the 12-MR channels. Dehydrogenation was thought to be especially affected because of its late and loose transition-state geometry, inferred from available density functional calculations. Monte Carlo simulations show that within MFI,[76] as in MOR,[77] *n*-butane is confined to different extents at different locations. An illustration of MFI, drawn in the plane of a sinusoidal channel, is presented in Figure 6. A

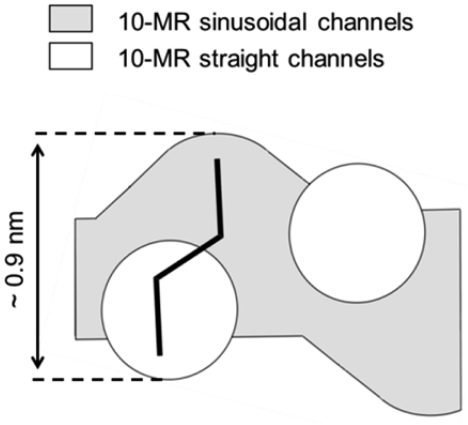

Figure 6. Illustration of channel environments in MFI. A molecule of *n*-butane is shown lying along a channel intersection.

butane molecule can orient along a straight or sinusoidal channel or, as shown in the figure, at an intersection where it is contained partly within a sinusoidal channel and protrudes into a straight channel perpendicularly.[76]

As noted already, the selectivity trends for MFI and for MOR (with respect to Al content and proton location, respectively) are similar. Moreover, we observe an increase in the rate coefficients with Al content (with the exception of MFI-11.5), a trend that was also observed with increasing the fraction of protons in the 8-MR of MOR. On the basis of these similarities,

dx.doi.org/10.1021/ja4081937 | J. Am. Chem. Soc. 2013, 135, 19193−19207

Table 6. Apparent Activation Enthalpies and Entropies for *n*-Butane Monomolecular Cracking and Dehydrogenation

		ΔH_{app} [a] (kJ mol^{-1})			ΔS_{app} [a,b] (J mol^{-1} K^{-1})		
zeolite	ref	central cracking	terminal cracking	dehydrogenation	central cracking	terminal cracking	dehydrogenation
MFI-140		137	143	189	−76	−73	−31
MFI-40		133	147	206	−78	−65	−2
MFI-25		128	147	208	−77	−57	14
MFI-15(P)		127	155	202	−73	−41	9
MFI-15(M)		133	161	205	−67	−34	13
MFI-11.5		133	156	198	−73	−47	−2
MFI-35	71	134	142	149	−72	−66	−77
	72	140[c]	140[c]	105	−64	−70	−130
	73, 74	135[c]	135[c]	115	−74	−79	−121
MFI-25[d]	24	–	150	200	–	−59	−6
MOR 8-MR	24	159	163	215	−42	−29	31
MOR 12-MR	24	134	–	–	−82	–	–

[a]Errors in activation energies and entropies for cracking are, respectively, ±5 kJ mol^{-1} and ±10 J mol^{-1} K^{-1}. Errors in activation energies and entropies for dehydrogenation are ±10 kJ mol^{-1} and ±15 J mol^{-1} K^{-1}. [b]Entropies of activation have been calculated from reported data using eqs 11−14. [c]Activation entropies and entropies correspond to cracking overall and not to individual central or terminal cracking pathways. [d]Propane used as reactant on H-MFI with a nominal Si/Al ratio of 25.

we propose that the effects of framework Al concentration on rates and selectivities in H-MFI are caused by changes in the distribution of Brønsted protons as the Al content increases, evidence for which was presented in Figure 2. It is therefore interesting that the rate coefficients for H-MFI increase with Al content up to 5.4 Al per unit cell and then decrease at the highest Al content (corresponding to MFI-11.5). It seems unlikely that this decrease is caused by a reduction in the acidity of protons as a result of the presence of next-nearest-neighbor (NNN) Al sites.[78−80] Such sequences have never been reported for MFI with Si/Al > 12 and have only been found in MFI with Si/Al ratios of 8.3−9.0,[19] consistent with the prediction by Barthomeuf that the Si/Al ratio required for Al NNN sites to appear in MFI is <9.5.[80] We also find it unlikely that a linear relationship would exist between *n*-hexane cracking activity and the Al concentration (for samples with Si/Al ratios ranging from 10 to several thousand), as reported by Haag and co-workers,[22,23] if the acidity of Brønsted protons in H-MFI varies strongly with the Al content. On the basis of the findings cited above, we propose that the downturn in the rate coefficient is related to differences in the concentration of the reactant state ($C_{A(r)}$) that result from changes in the values of K_H and p_r and, by extension, K_{ads} (see eqs 6 and 10). These parameters are functions of proton location and, therefore, likely contribute partly to the observed variation in the apparent rate coefficients (see Supporting Information). This proposal is reasonable because, as seen in Figure 2, the distribution of Co(II) cations (and, by extension, protons) differs between MFI-15 and MFI-11.5, even though the fraction of Co(II) located at intersections is similar.

Thus far we have presented evidence that trends in the apparent rates and selectivities of *n*-butane cracking and dehydrogenation with respect to Al content in H-MFI are caused by underlying variation in the spatial distribution of Brønsted protons and are influenced by changes in the intrinsic rate coefficients. Information on the enthalpic and entropic driving forces behind these trends can be inferred from the experimental activation parameters and transition-state geometries and provides a basis for interpreting the relative kinetic preferences of *n*-butane cracking and dehydrogenation to occur at different structural environments. The apparent activation energies and entropies calculated using eqs 13 and 14 are given in Table 6 and are plotted versus the Al content in Figure 7. For comparison, values of the activation parameters reported in previous experimental studies[24,71−74] are also given in Table 6. The experimentally measured activation energies for central cracking and terminal cracking agree well with values reported

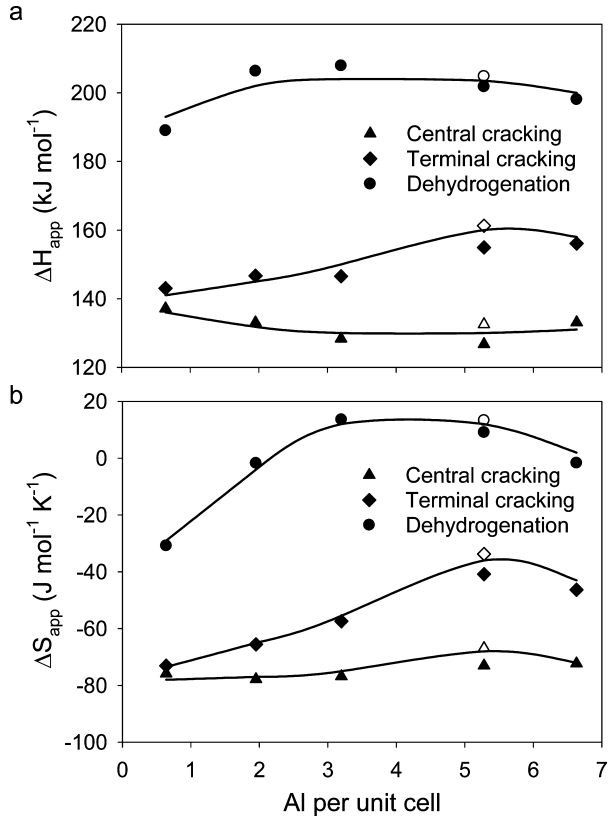

Figure 7. Apparent activation enthalpies and entropies of *n*-butane monomolecular cracking and dehydrogenation versus Al atoms per unit cell in MFI. Data for MFI-15(M), which was treated with EDTA, are indicated with hollow symbols. Errors in activation energies and entropies for cracking are, respectively, ± 5 kJ mol^{-1} and ± 10 J mol^{-1} K^{-1}. Errors in activation energies and entropies for dehydrogenation are ± 10 kJ mol^{-1} and ± 15 J mol^{-1} K^{-1}.

dx.doi.org/10.1021/ja4081937 | J. Am. Chem. Soc. 2013, 135, 19193−19207

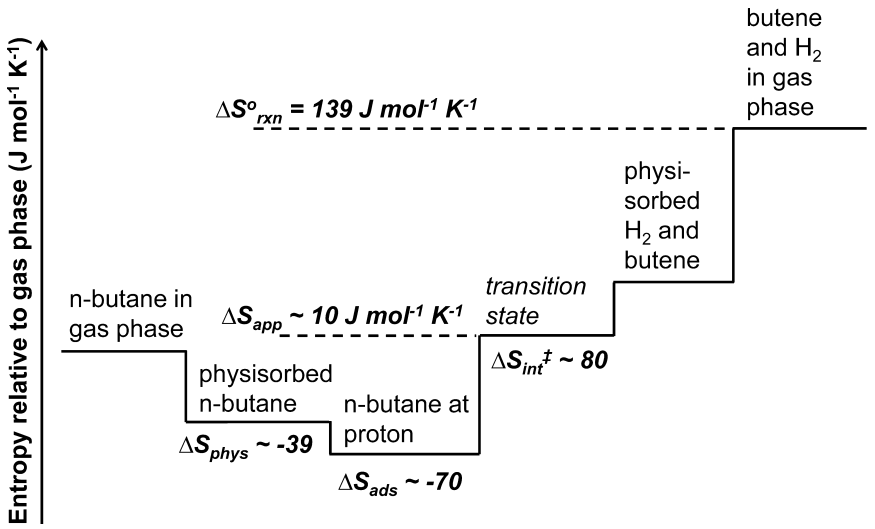

Figure 8. Illustration of the entropy changes involved in the elementary steps of monomolecular reactions of alkanes over acidic zeolites. Entropy values are indicated in the diagram for the dehydrogenation of *n*-butane. The standard entropy of reaction $\Delta S°_{rxn}$ has been extrapolated to 773 K from standard entropies of formation of *n*-butane, hydrogen and 1-butene at 1 bar and 298 K taken from ref 62.

previously for MFI. The activation energies for dehydrogenation agree with experimental values reported for *n*-butane dehydrogenation on MOR and propane dehydrogenation on MFI,[24] and with theoretical values for *n*-butane dehydrogenation on MFI.[81] However, our values for the apparent activation energies of *n*-butane dehydrogenation (189−208 kJ mol^{-1}) are considerably higher than other experimental values for *n*-butane dehydrogenation on MFI (115−149 kJ mol^{-1}). As discussed in the Supporting Information, the activation barrier for dehydrogenation is sensitive to whether the rate coefficients used to construct the Arrhenius plot for this process were measured at fixed space time or extrapolated to zero space time. For example, in the case of MFI-11.5, we obtained an activation barrier of 198 kJ mol^{-1} on the basis of rate coefficients that were extrapolated to zero space time, and a value of 149 kJ mol^{-1} was obtained if a fixed space time of 0.39 [s (mol H^+) (mol feed)$^{-1}$] was used. The difference in the two values of the activation energy is attributable to the influence of inhibition by isobutene (see section 3.5), which becomes more severe as the space time and, concomitantly, the isobutene partial pressure increase. While a strong preference for methylene versus methyl C−H activation[81] or strong Lewis acidity[43] could also cause the lower activation barriers reported in the literature, it is notable that the values of the apparent activation energy that we have obtained by measuring rates at fixed space time agree well with the previously reported values.

Figure 7 shows that the activation energy and entropy for terminal cracking increase with the Al content up to 5.4 Al per unit cell and then decrease at the highest Al content of 7.3 Al per unit cell. The apparent activation energy and entropy for this reaction span ranges of 18 kJ mol^{-1} and 39 J mol^{-1} K^{-1}, respectively. These ranges are larger than the estimated spread in the magnitudes of ΔH_{ads} (<14 kJ mol^{-1})[70] and ΔS_{ads} (<14 J mol^{-1} K^{-1}) for the adsorption of *n*-butane from the gas phase into different locations within MFI (see Supporting Information). On the basis of eqs 13 and 14, this result suggests that the trends in the apparent activation energy and entropy with Al content for terminal cracking reflect trends in the intrinsic activation energy and entropy. This conclusion can also be reached for *n*-butane dehydrogenation because values of E_{app} and ΔS_{app} differ, respectively, by up to 19 kJ mol^{-1} and 45 J mol^{-1} K^{-1}. On the other hand, E_{app} and ΔS_{app} for central cracking are similar within experimental error. The identification of subtle trends in the activation parameters for this reaction is, therefore, difficult. From these results it appears that neither the intrinsic activation energies, nor the differences between intrinsic activation energies of different reactions, are constant. This might be anticipated from density functional calculations in which the intrinsic activation enthalpy for a given activation reaction of *n*-butane was found to differ by up to 21 kJ mol^{-1} for different active site locations within MFI.[81] These findings differ from those reported previously in which it was concluded that the intrinsic activation energy is constant for a given bond cleavage reaction and that differences between activation energies are determined by differences in the proton affinities of gas phase reactant molecules protonated at specific C−C and C−H bonds.[24,30] The proposal that intrinsic activation energies and entropies for dehydrogenation and terminal cracking increase with Al content in MFI is consistent with the conclusion that trends in the apparent rate coefficients with Al content reflect changes in the intrinsic rate coefficients. As discussed below, these changes in rates are driven by changes in the entropies of activation.

It can be seen by comparing Figures 4 and 7 that the rate coefficient for terminal cracking increases with the Al content despite concurrent increases in the activation energy. This result indicates that the change in activation entropy for terminal cracking has a greater effect on the Gibbs free energy of activation than the change in activation energy. The rate coefficient for dehydrogenation also increases with Al content despite similar or increasing values of the activation energy; the value of E_{app} increases between 1 and 2 Al per unit cell and then remains similar for higher Al contents. This result signals that entropy effects are also dominant for the dehydrogenation. As noted above, the trends observed in the activation parameters for dehydrogenation and terminal cracking with Al content are influenced by changes in the intrinsic activation energies and entropies. This then implies that increases in the rate coefficients originate at least partly from increases in the intrinsic activation entropies that offset increases in the intrinsic activation energies. We propose that a larger fraction of protons located at channel intersections at higher Al content causes a

dx.doi.org/10.1021/ja4081937 | J. Am. Chem. Soc. 2013, 135, 19193−19207

decrease in the confinement of transition states and an increase in both the apparent and intrinsic activation entropies. This suggestion is consistent with the greater activation energies observed at higher Al content for dehydrogenation and terminal cracking, because reactants and transition states that are less confined are also less stabilized enthalpically. It is therefore interesting that the rate coefficient of central cracking appears to be correlated with both a decrease in the activation energy and a slight increase in the activation entropy (see Figures 4 and 7), although as noted, the variations in these quantities are close in magnitude to their respective uncertainties. However, a decrease in the activation energy for central cracking with the Al content is not necessarily inconsistent with the proposal that the transition state is becoming less confined. Mallikarjun Sharada et al. have calculated two distinct transition states for central cracking, which have activation enthalpies that differ by 27 kJ mol^{-1}.[81] A greater preference at higher Al content to populate the transition state that has the lower activation enthalpy would cause the apparent activation energy to decrease even if the transition state were less confined.

Concurrent changes in the apparent activation energy and entropy for a given elementary reaction in zeolites can be anticipated as a consequence of changes in the confinement of reactants and transition states. As the space surrounding the Brønsted acid sites decreases, the reactant and the transition state can be stabilized more by the O atoms of the zeolite framework. As seen in Figure 3, increasing the enthalpic stabilization of reactant and transition states causes the apparent activation energy to decrease. Furthermore, Table 6 shows that for the central cracking of *n*-butane on MOR, the apparent activation energy is 25 kJ mol^{-1} smaller when protons are located in the 12-MR channels than in the 8-MR side pockets. On the other hand, increasing the confinement lowers the entropy of reactants and transition states, as illustrated in Figure 8. Thus, the apparent activation entropy at the 8-MR locations is 40 J mol^{-1} K^{-1} higher than at the 12-MR locations. If changes in E_{app} and ΔS_{app} that result from changes in the environment of Brønsted protons differ from the corresponding changes in enthalpy and entropy of adsorption (ΔH_{ads} and ΔS_{ads}), as we have suggested, then the intrinsic energy and entropy of activation ($E^{\ddagger}_{int}$ and $\Delta S^{\ddagger}_{int}$) must change with the confinement. The degree to which changes in transition-state confinement affect $\Delta S^{\ddagger}_{int}$ is likely to be due to whether the transition state is early or late along the reaction coordinate, because of the generation of translational and rotational modes that occur as a result of the transformation of one molecule into two. By this reasoning, early transition states, which resemble the reactant state more closely than the product state, would be affected to a lesser degree by changes in confinement than late transition states, which resemble the product state more closely.

The geometries of the transition states for *n*-butane dehydrogenation and cracking at Brønsted acid sites associated with Al at T10 and T12 have been reported recently by Mallikarjun Sharada et al.[81] The transition state structure for *n*-butane dehydrogenation comprises a nearly free hydrogen molecule and a butyl cation fragment that releases a proton to a zeolite oxygen atom. It is, therefore, reasonable to characterize the transition state for dehydrogenation as late. By contrast, the transition states for central and terminal cracking more closely resemble pentacoordinated carbonium ions. In central cracking, however, the molecule interacts more closely with the zeolite because even the methyl ends must be brought close to the framework. Central cracking might therefore be expected to exhibit a lower intrinsic activation entropy and a lower preference for less confining locations in MFI as a consequence of the closer overall proximity to the framework. The proposed classification of transition states for *n*-butane dehydrogenation and cracking are qualitatively consistent with the relative magnitudes of the activation entropies reported in Table 6 and the sensitivity of activation entropies to Al concentration. In all cases, the apparent activation entropy remains similar or becomes less negative as the framework concentration of Al increases, i.e., as the fraction of Co(II) present in β-sites located at the channel intersections increases. This effect is strongest for late transition states (e.g., dehydrogenation) and is weaker for transition states that are earlier (e.g., cracking), especially those such as central tracking, where the transition state is more constrained to the zeolite framework.

3.4. Analysis of Rotational and Translational Components of Intrinsic Activation Entropies. An examination of intrinsic activation entropies, given below, provides further support for the proposal that transition states differ in terms of their interactions with the zeolite and their positions along the reaction coordinate. It is useful to begin this discussion by examining the entropy changes involved relative to the gas phase for the dehydrogenation of *n*-butane, as diagrammed in Figure 8. The entropy of adsorption from the gas phase to the reactant state, ΔS_{ads} (~ -70 J mol^{-1} K^{-1}), is equal to the sum of ΔS_{phys} and the entropy lost upon localization at a proton (ΔS_r). In order to calculate the intrinsic activation entropy from eq 13, the value of ΔS_r must be estimated. Using the equations outlined in section 3.2, ΔS_r can be expressed as

$$\Delta S_r = \frac{\Delta H_r}{T} + R \ln\left[p_r \times \frac{V_{pore}}{V_{H^+}}\right] \quad (15)$$

Simulations show that values of p_r for silicalite are independent of temperature under the conditions of the experiments because ΔH_r is near zero.[63] To be consistent with the conditions for which p_r was calculated, ΔH_r in eq 15 is set to zero in order to estimate ΔS_r, even though there is a decrease in enthalpy ($\sim$7–10 kJ mol^{-1}) associated with the specific interaction of the alkane with a proton.[64,65] Values of p_r for central and terminal C–C bonds were taken from ref 63. An average value of p_r for dehydrogenation was estimated by assuming that methylene and methyl C–H bonds have the same values for p_r as central and terminal C–C bonds, respectively. The intrinsic activation entropies were then calculated using the apparent activation entropies along with eqs 13 and 15, and are presented in Table 7. It can be seen that the dehydrogenation activation entropies are exclusively positive, whereas for central cracking the activation entropies

Table 7. Intrinsic Activation Entropies of Monomolecular *n*-Butane Cracking and Dehydrogenation Reactions

	$\Delta S^{\ddagger}_{int}$ (J mol^{-1} K^{-1})		
zeolite	central cracking	terminal cracking	dehydrogenation
MFI-140	−17	−16	27
MFI-40	−19	−8	56
MFI-25	−18	0	71
MFI-15(P)	−15	16	67
MFI-15(M)	−8	24	71
MFI-11.5	−15	10	55

dx.doi.org/10.1021/ja4081937 | J. Am. Chem. Soc. 2013, 135, 19193–19207

are weakly negative, and values for terminal cracking span a range of small negative and positive values. The strongly positive activation entropies for dehydrogenation are consistent with the creation of rotational and translational entropy at the transition state, and the channel intersections are the most obvious environments within MFI that permit access to these modes.

In order to rationalize the magnitudes of the intrinsic activation entropy, the changes in rotational and translational entropy between the reactant state and the fully formed products of dehydrogenation (assuming 1-butene for the product alkene) were calculated using methods of statistical mechanics similar to those described by previous authors[30] (see Supporting Information). The estimation of the translational entropy requires the specification of a length, area or volume over which the translation can occur. We have chosen to use the diameter, largest cross sectional area, and volume of the largest included sphere calculated by Foster and co-workers[82] for MFI, for 1D, 2D, and 3D translation, respectively. This sphere is situated at the channel intersection and values of its diameter, cross sectional area and volume are included in Table 8. The rotational and translational entropy change of the dehydrogenation reaction was then estimated for the case of 1D free rotation of H_2 and differing degrees of rotational and translational motion of 1-butene. In all cases considered, 1D translation along a distance of 6.30 Å and 1D free rotation were assumed for the *n*-butane reactant. Three different scenarios were considered in order to approximate the entropic effect of the stronger electrostatic interaction of a butyl cation-like fragment with the framework relative to the interaction of the neutral reactant. First, rotational and translational contributions to the 1-butene entropy were neglected. In a second treatment, the 1-butene was considered to possess 1D free rotation, consistent with the assumption made for *n*-butane. It is presumed that 1D rotation could be achieved without strongly influencing the electrostatic stabilization of the butyl fragment, provided that the distance of this fragment from the zeolite oxygen remains unperturbed by the rotation. Finally, 1D translational motion of butene is permitted in addition to 1D rotation, but the distance over which the translation can occur is limited to 1 Å, considerably less than the distance of 6.30 Å permitted for the neutral reactant molecule. The results of performing these calculations are summarized in Table 8. The intrinsic activation entropies extracted from experimental data in Table 7 fall within the ranges of values estimated from statistical mechanics for 1D, 2D, or 3D translation of H_2, provided that some rotation and translation is contributed from the butyl fragment. The comparison indicates that free or frustrated translations and rotations of product fragments contribute strongly to the entropy and free energy of the dehydrogenation transition state.

Table 8. Changes in Rotational and Translational Entropy (J mol^{-1} K^{-1}) at 773 K for Dehydrogenation of *n*-Butane To Produce H_2 and 1-Butene Assuming 1D Free Rotation of H_2[a]

H_2 translation		C_4H_8 rotation and translation		
dimensionality	allowed space[b]	none	1D rotation	1D rotation and 1D translation[c]
1D	$2R$ (6.3 Å)	−37	−1	33
2D	πR^2 (31 Å^2)	−13	24	57
3D	$4\pi R^3/3$ (131 Å^3)	10	47	80

[a]Translation over a linear distance of 6.3 Å and 1D free rotation are assumed for *n*-butane. [b]Spaces available for 1D, 2D, or 3D translation are given in terms of the radius R of the largest sphere included within the channel intersection, 3.15 Å.[82] [c]Lengths allowed for translation of 1-butene and *n*-butane are, respectively, 1.0 and 6.3 Å.

3.5. Inhibitory Effects of Isobutene on Rates of *n*-Butane Reactions. Figure 9a shows the rates of product formation resulting from *n*-butane cracking and dehydrogenation via monomolecular processes on MFI-11.5 at 773 K as functions of the butene partial pressure. The partial pressure of butene in the effluent was varied by changing the partial pressure of *n*-butane at a fixed total flow rate. It can be seen that the rate of *n*-butane dehydrogenation (H_2 and butenes) decreases noticeably as the partial pressure of butene increases, suggesting that dehydrogenation is inhibited by the presence of butene. As discussed below, the observed decrease in the rate of dehydrogenation cannot be attributed to inhibition by propene or, by extension, ethene, since the addition of propene to the feed had no effect on the rates. Figure 9a also shows that the rates of formation of propane and isobutane, formed via bimolecular hydride transfer from *n*-butane to propene and isobutene,[83−85] decrease with increasing partial pressure of

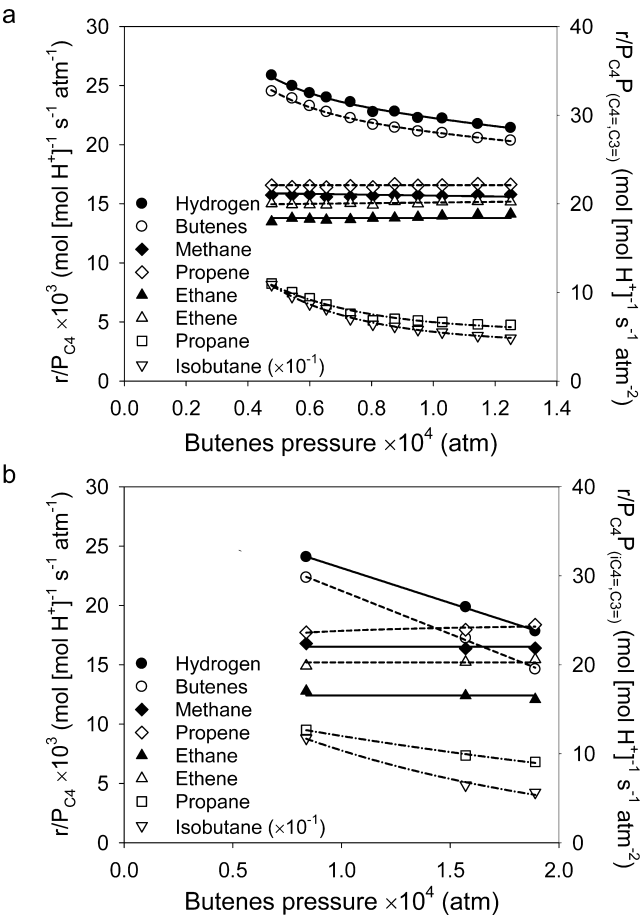

Figure 9. (a) Rates of monomolecular reactions (left axis) and secondary hydride transfer reactions (right axis) versus butene partial pressure for MFI-11.5 at 773 K and a space time of 0.09 [s (mol H$^+$) (mol feed)$^{-1}$]. Conversion is constant at 0.57 ± 0.02 %. (b) Rates of reactions as stated in (a), but with varying levels of isobutene introduced as co-feed. Horizontal axis indicates the total partial pressure of butenes.

dx.doi.org/10.1021/ja4081937 | J. Am. Chem. Soc. 2013, 135, 19193−19207

butene. The products produced by a given monomolecular reaction pathway (e.g., C_2H_6 and C_2H_4 for central cracking) are formed at nearly equal rates, and hydrocarbons larger than C_4 are not observed above trace levels. Therefore, decreases in the rates of appearance of these products cannot be attributed to secondary conversion. In addition, the rate measurements are taken far below the equilibrium conversion for dehydrogenation, which is 49% at reaction conditions (for 1-butene as the alkene product). Therefore, an approach to equilibrium does not influence the measured rates, leaving product inhibition as the most plausible explanation for the reduction in reaction rates of *n*-butane. Further support for this hypothesis is presented in Figure 9b, which shows that the changes in rates of *n*-butane dehydrogenation and hydride transfer seen in Figure 9a can be reproduced qualitatively by introducing isobutene to the feed without changing the partial pressure of *n*-butane. Reaction rates returned to their starting values after the co-feed was removed, consistent with a reversible adsorption process. Co-feeding propene had no detectable influence on the kinetics of any reactions (see Supporting Information). We, therefore, surmise that the decreases in *n*-butane reaction rates shown in Figure 9 are caused by the adsorption of one or more butene isomers onto Brønsted protons. However, because these isomers equilibrate rapidly, the inhibition cannot be attributed to a specific species based solely on the data shown. As discussed in detail in the Supporting Information, we have combined experimental estimates of the thermodynamic adsorption parameters for butene adsorption with density functional calculations in order to gain insight as to the identity of the inhibiting species.

The Gibbs free energy of adsorption for butene, ΔG°_{ads}, was extracted from values of the Langmuir coefficient that were obtained from linearized fits of the rate data taken at different levels of isobutene co-feed. The adsorption enthalpy (ΔH°_{ads}) was then calculated theoretically for adsorption at the intersection and sine channel in MFI. The entropy of adsorption ΔS°_{ads} was estimated for these locations by using the results of theoretical work reported by De Moor et al.,[86] who modeled the low-energy vibrations of adsorbed molecules as rotations and translations in order to calculate the entropy of adsorption onto a proton in a zeolite. Feasible combinations of ΔS°_{ads} and ΔH°_{ads} must then satisfy the constraint $\Delta G^\circ_{ads} = \Delta H^\circ_{ads} - (773\ \mathrm{K})(\Delta S^\circ_{ads})$. Our analysis suggests that this constraint is met by the adsorption of isobutene in the intersections of H-MFI, but not by the adsorption of isobutene in the channels or by linear butenes in general. Taken together with the selectivity of the inhibition for dehydrogenation, these results support the earlier proposal that dehydrogenation exhibits a greater preference than cracking to occur at intersections in MFI. Also, the lack of an effect of butene on the rates of cracking (within the range of butene partial pressures studied) seems to indicate that this preference is quite strong, and that the fraction of Brønsted protons located directly at the channel intersections is relatively small.

The analysis given above has several implications. First, the reasonable agreement of the experimentally estimated and theoretically calculated adsorption parameters supports the hypothesis that alkene inhibition is possible even at the low conversions used for this work. For this reason, rate coefficients should be extrapolated to zero conversion or extracted from kinetic models that account for product readsorption. Obtaining rates at a fixed space time across different temperatures may result in an artificially low value of the activation energy as discussed above. It is also significant that the rates of dehydrogenation and hydride transfer are inhibited simultaneously. As originally proposed by Haag and Dessau[1] and supported by subsequent experimental studies,[87] the relatively bulky bimolecular transition state for the rate-determining step in hydride transfer is formed more easily in larger pore environments. The simultaneous inhibition of both processes in H-MFI, therefore, implies that each reaction exhibits a strong kinetic preference for channel intersections.

4. CONCLUSIONS

Rate coefficients, activation parameters and selectivities for the monomolecular cracking and dehydrogenation of *n*-butane were obtained for MFI samples obtained from a single source, with Si/Al ratios ranging from 12 to 142 (0.7−7.3 Al atoms per unit cell). The rate of dehydrogenation relative to cracking and the rate of terminal cracking relative to central cracking increased with increasing Al content. The rates of all three reactions increased with increasing Al content up to 5.4 Al atoms per unit cell and then decreased at the highest Al content. The increase in rates occurred despite similar or increasing activation energies, and is caused partly by increases in the activation entropy. We suggest that these effects are consequences of an increased fraction of protons being located in less confining portions of the zeolite pore system (e.g., channel intersections) as the Al content increases. Based on calculated transition-state geometries and values of the intrinsic activation entropies extracted from experimental data, the anticipated order of preference of the different reactions for less confining locations is dehydrogenation > terminal cracking > central cracking. The increased selectivities to terminal cracking and to dehydrogenation at higher Al content support the proposed trend in the distribution of Al. The suggested trends in Al distribution are also consistent with trends in the locations of Co(II) inferred from UV−visible spectra, which show that more Co(II) was located at the intersections as the Al concentration increased. Unexpectedly, butene was found to influence the measured activation energies for dehydrogenation if rates were not extrapolated to zero space time in order to achieve very low product partial pressures. QM/MM calculations suggest that the inhibition is due primarily to isobutene adsorbed in the channel intersections.

In summary, we conclude from the analysis of reaction rate measurements and spectroscopic data that the fraction of Al in the intersections of H-MFI increases with increasing Al content. Terminal cracking and dehydrogenation of *n*-butane occur preferentially on Brønsted acid protons located at channel intersections because of the higher intrinsic entropies of activation and consequently lower Gibbs free energies attainable at these sites. The higher intrinsic activation entropies appear to override the effects of higher intrinsic activation energies, most noticeably for terminal cracking and dehydrogenation. Therefore, the results of this study indicate that intrinsic activation energies are not constant, and that differences between activation barriers for various monomolecular reactions are a function of the location of Brønsted protons. The results also suggest that the ratio of terminal to central cracking and the ratio of cracking to dehydrogenation of butane can be controlled indirectly by varying the Al content of the zeolite framework.

dx.doi.org/10.1021/ja4081937 | J. Am. Chem. Soc. 2013, 135, 19193−19207

■ ASSOCIATED CONTENT

Supporting Information

Transient rate data, FTIR spectra, analyses and calculations of thermodynamic adsorption parameters, and details of statistical mechanical calculations. This material is available free of charge via the Internet at http://pubs.acs.org.

■ AUTHOR INFORMATION

Corresponding Author

bell@cchem.berkeley.edu

Notes

The authors declare no competing financial interest.

■ ACKNOWLEDGMENTS

This work was carried out with financial support from Chevron Energy Technology Company and an NDSEG fellowship awarded by the American Society for Engineering Education. The authors also thank Joseph Gomes and Dr. Joseph Swisher for providing QM/MM and Monte Carlo simulations, respectively, and for useful discussion.

■ REFERENCES

(1) Haag, W. O.; Dessau, R. M. *Proceedings of the 8th International Congress on Catalysis*, Berlin; Verlag Chemie: Weinheim, 1984; Vol. 2, p 305.

(2) Kotrel, S.; Knözinger, H.; Gates, B. C. *Microporous Mesoporous Mater.* **2000**, *35*−*36*, 11.

(3) Konno, H.; Okamura, T.; Kawahara, T.; Nakasaka, Y.; Tago, T.; Masuda, T. *Chem. Eng. J. (Amsterdam, Neth.)* **2012**, *207*−*208*, 490.

(4) Voogd, P.; van Bekkum, H. *Appl. Catal.* **1990**, *59*, 311.

(5) Haag, W. O.; Lago, R. M.; Weisz, P. B. *Faraday Discuss. Chem. Soc.* **1982**, *72*, 317.

(6) Han, O. H.; Kim, C. S.; Hong, S. B. *Angew. Chem., Int. Ed.* **2002**, *41*, 469.

(7) Dědeček, J.; Kaucký, D.; Wichterlová, B. *Microporous Mesoporous Mater.* **2000**, *35*−*36*, 483.

(8) Dědeček, J.; Kaucký, D.; Wichterlová, B. *Chem. Commun.* **2001**, 970.

(9) Wichterlová, B.; Dědeček, J.; Sobalík, Z.; Čejka, J. *Stud. Surf. Sci. Catal.* **2001**, *135*, 344.

(10) Dědeček, J.; Kaucký, D.; Wichterlová, B.; Gonsiorová, O. *Phys. Chem. Chem. Phys.* **2002**, *4*, 5406.

(11) Dědeček, J.; Čejka, J.; Oberlinger, M.; Ernst, S. *Stud. Surf. Sci. Catal.* **2002**, *142*, 23.

(12) Dědeček, J.; Balgová, V.; Pashková, V.; Klein, P.; Wichterlová, B. *Chem. Mater.* **2012**, *24*, 3231.

(13) Gábová, V.; Dědeček, J.; Čejka, J. *Chem. Commun.* **2003**, 1196.

(14) Abraham, A.; Lee, S.-H.; Shin, C.-H.; Hong, S. B.; Prins, R.; van Bokhoven, J. A. *Phys. Chem. Chem. Phys.* **2004**, *6*, 3031.

(15) Sklenak, S.; Dědeček, J.; Li, C.; Wichterlová, B.; Gábová, V.; Sierka, M.; Sauer, J. *Angew. Chem., Int. Ed.* **2007**, *46*, 7286.

(16) Sklenak, S.; Dědeček, J.; Li, C.; Wichterlová, B.; Gábová, V.; Sierka, M.; Sauer, J. *Phys. Chem. Chem. Phys.* **2009**, *11*, 1237.

(17) Pinar, A. B.; Márquez-Álvarez, C.; Grande-Casas, M.; Pérez-Pariente, J. *J. Catal.* **2009**, *263*, 258.

(18) Román-Leshkov, Y.; Moliner, M.; Davis, M. E. *J. Phys. Chem. C* **2011**, *115*, 1096.

(19) Dědeček, J.; Sobalík, Z.; Wichterlová, B. *Catal. Rev.: Sci. Eng.* **2012**, *54*, 135.

(20) Lu, B.; Kanai, T.; Oumi, Y.; Sano, T. *J. Porous Mater.* **2007**, *14*, 89.

(21) Olson, D. H.; Haag, W. O.; Lago, R. M. *J. Catal.* **1980**, *61*, 390.

(22) Haag, W. O.; Lago, R. M.; Weisz, P. B. *Nature* **1984**, *309*, 539.

(23) Haag, W. O. *Stud. Surf. Sci. Catal.* **1994**, *84*, 1375.

(24) Gounder, R.; Iglesia, E. *J. Am. Chem. Soc.* **2009**, *131*, 1958.

(25) Parrillo, D. J.; Lee, C.; Gorte, R. J. *Appl. Catal., A* **1994**, *110*, 67.

(26) Auroux, A.; Gravelle, P. C.; Védrine, J. C.; Reka, M. *Proceedings of the 5th International Zeolite Conference*, Naples; Heyden: London/Philadelphia/Rheine, 1980; p 433.

(27) Sazama, P.; Dědeček, J.; Gábová, V.; Wichterlová, B.; Spoto, G.; Bordiga, S. *J. Catal.* **2008**, *254*, 180.

(28) Eichler, U.; Brändle, M.; Sauer, J. *J. Phys. Chem. B* **1997**, *101*, 10035.

(29) Sauer, J.; Sierka, M. *J. Comput. Chem.* **2000**, *21*, 1470.

(30) Gounder, R.; Iglesia, E. *Acc. Chem. Res.* **2012**, *45*, 229.

(31) de Boer, J. H.; Lippens, B. C.; Linsen, B. G.; Broeckhoff, J. C. P.; van den Heuvel, A.; Onsinga, T. V. *J. Colloid Interface Sci.* **1966**, *21*, 405.

(32) Harkins, W. D.; Jura, G. *J. Am. Chem. Soc.* **1944**, *66*, 1366.

(33) Gounder, R.; Jones, A. J.; Carr, R. T.; Iglesia, E. *J. Catal.* **2012**, *28*, 214.

(34) Liu, D.; Bhan, A.; Tsapatsis, M.; Al Hashimi, S. *ACS Catal.* **2011**, *1*, 7.

(35) Cheung, P.; Bhan, A.; Sunley, G. J.; Law, D. J.; Iglesia, E. *J. Catal.* **2007**, *245*, 110.

(36) Joly, J. F.; Zanier-Szydlowski, N.; Colin, S.; Raatz, F.; Saussey, J.; Lavalley, J. C. *Catal. Today* **1991**, *9*, 31.

(37) Parry, E. P. *J. Catal.* **1963**, *2*, 371.

(38) Maier, S. M.; Jentys, A.; Lercher, J. A. *J. Phys. Chem. C* **2011**, *115*, 8005.

(39) Drozdová, L.; Prins, R.; Dědeček, J.; Sobalík, Z.; Wichterlová, B. *J. Phys. Chem. B* **2002**, *106*, 2240.

(40) Li, S.; Zheng, A.; Su, Y.; Zhang, H.; Chen, L.; Yang, J.; Ye, C.; Deng, F. *J. Am. Chem. Soc.* **2007**, *129*, 11161.

(41) Marques, J. P.; Gener, L.; Ayrault, P.; Lopes, J. M.; Ribeiro, F. R.; Guisnet, M. *Chem. Commun.* **2004**, 2290.

(42) Gola, A.; Rebours, B.; Milazzo, E.; Lynch, J.; Benazzi, E.; Lacombe, S.; Delevoye, L.; Fernandez, C. *Microporous Mesoporous Mater.* **2000**, *40*, 73.

(43) Al-Majnouni, K. A.; Yun, J. H.; Lobo, R. F. *ChemCatChem* **2011**, *3*, 1333.

(44) Voogd, P.; Scholten, J. J. F.; van Bekkum, H. *Colloids Surf.* **1991**, *55*, 163.

(45) Hudec, P.; Smieskova, A.; Zidek, Z.; Zubek, M.; Schneider, P.; Kocirik, M.; Kozankova, J. *Collect. Czech. Chem. Commun.* **1998**, *63*, 141.

(46) Janssen, A. H.; Schmidt, I.; Jacobsen, C. J. H.; Koster, A. J.; de Jong, K. P. *Microporous Mesoporous Mater.* **2003**, *65*, 59.

(47) Müller, U.; Unger, K. K. *Stud. Surf. Sci. Catal.* **1988**, *39*, 101.

(48) Müller, U.; Reichert, H.; Robens, E.; Unger, K. K.; Grillet, Y.; Rouquerol, F.; Rouquerol, J.; Pan, D.; Mersmann, A. *Fresenius Z. Anal. Chem.* **1989**, *333*, 433.

(49) Groen, J. C.; Peffer, L. A. A.; Pérez-Ramírez, J. *Microporous Mesoporous Mater.* **2003**, *60*, 1.

(50) Saito, A.; Foley, H. *Microporous Mater.* **1995**, *3*, 543.

(51) Kubelková, L.; Beran, S.; Małecka, A.; Mastikhin, V. M. *Zeolites* **1989**, *9*, 12.

(52) Kuehl, G. H. *J. Phys. Chem. Solids* **1977**, *38*, 1259.

(53) Gonzalez, M. R.; Sharma, S. B.; Chen, D. T.; Dumesic, J. A. *Catal. Lett.* **1993**, *18*, 183.

(54) Datka, J.; Marschmeyer, S.; Neubauer, T.; Meusinger, J.; Papp, H.; Schütze, F.-W.; Szpyt, I. *J. Phys. Chem.* **1966**, *100*, 14451.

(55) Loeffler, E.; Lohse, U.; Peuker, Ch.; Oehlmann, G.; Kustov, L. M.; Zholobenko, V. L.; Kazansky, V. B. *Zeolites* **1990**, *10*, 266.

(56) Guisnet, M.; Ayrault, P.; Coutanceau, C.; Alvarez, M. F.; Datka, J. *J. Chem. Soc., Faraday Trans. 1* **1997**, *93*, 1661.

(57) Marques, J. P.; Gener, I.; Ayrault, P.; Bordado, J. C.; Lopes, J. M.; Ribeiro, F. R.; Guisnet, M. *C.R. Chimie* **2005**, *8*, 399.

(58) Aramburo, L. R.; Karwacki, L.; Cubillas, P.; Asahina, S.; de Winter, D. A. M.; Drury, M. R.; Buurmans, I. L. C.; Stavitski, E.; Mores, D.; Daturi, M.; Bazin, P.; Dumas, P.; Thibault-Starzyk, F.; Post, J. A.; Anderson, M. W.; Terasaki, O.; Weckhuysen, B. M. *Chem.—Eur. J.* **2011**, *17*, 13773.

(59) Wichterlová, B.; Dědeček, J.; Sobalík, Z. In *Catalysis by Unique Metal Ion Structures in Solid Matrices: from Science to Application*; Centi,

G., Wichterlová, B., Bell, A. T., Eds.; NATO Science Series II; Kluwer Academic Publishers: Dordrecht, 2001; Vol. *13*, p 31.
(60) Sobalík, Z.; Dědeček, J.; Kaucký, D.; Wichterlová, B.; Drozdová, L.; Prins, R. *J. Catal.* **2000**, *194*, 330.
(61) Rice, M. J.; Chakraborty, A. K.; Bell, A. T. *J. Catal.* **1999**, *186*, 222.
(62) Stull, D. R.; Westrum, E. F.; Sinke, G. C. *The Chemical Thermodynamics of Organic Compounds*; Wiley: New York, 1987.
(63) Swisher, J. A.; Hansen, N.; Maesen, T.; Keil, F. J.; Smit, B.; Bell, A. T. *J. Phys. Chem. C* **2010**, *114*, 10229.
(64) Eder, F.; Lercher, J. A. *Zeolites* **1997**, *18*, 75.
(65) Titiloye, J. O.; Parker, S. C.; Stone, F. S.; Catlow, C. R. A. *J. Phys. Chem.* **1991**, *95*, 4038.
(66) First, E. L.; Gounaris, C. E.; Wei, J.; Floudas, C. A. *Phys. Chem. Chem. Phys.* **2011**, *13*, 17339.
(67) Savara, A.; Schmidt, C. M.; Geiger, F. M.; Weitz, E. *J. Phys. Chem. C* **2009**, *113*, 2806.
(68) Donaldson, D. J.; Ammann, M.; Bartels-Rausch, T.; Pöschl, U. *J. Phys. Chem. A* **2012**, *116*, 6312.
(69) Savara, A. *J. Phys. Chem. C* **2013**, *117*, 15710.
(70) De Moor, B. A.; Reyniers, M.-F.; Gobin, O. C.; Lercher, J. A.; Marin, G. B. *J. Phys. Chem. C* **2011**, *115*, 1204.
(71) Krannila, H.; Haag, W. O.; Gates, B. C. *J. Catal.* **1992**, *135*, 115.
(72) Lercher, J. A.; van Santen, R. A.; Vinek, H. *Catal. Lett.* **1994**, *27*, 91.
(73) Narbeshuber, T. F.; Vinek, H.; Lercher, J. A. *J. Catal.* **1995**, *157*, 388.
(74) Narbeshuber, T. F.; Brait, A.; Seshan, K.; Lercher, J. A. *J. Catal.* **1997**, *172*, 127.
(75) Arik, I. C.; Denayer, J. F.; Baron, G. V. *Microporous Mesoporous Mater.* **2003**, *60*, 111.
(76) Smit, B.; Siepmann, J. I. *J. Phys. Chem.* **1994**, *98*, 8442.
(77) Bates, S. P.; van Well, W. J. M.; van Santen, R. A. *J. Phys. Chem.* **1996**, *100*, 17573.
(78) Dempsey, E. *J. Catal.* **1974**, *33*, 497.
(79) Dempsey, E. *J. Catal.* **1975**, *39*, 155.
(80) Barthomeuf, D. *Mater. Chem. Phys.* **1987**, *17*, 49.
(81) Mallikarjun Sharada, S.; Zimmerman, P. M.; Bell, A. T.; Head-Gordon, M. *J. Phys. Chem. C* **2013**, *117*, 12600.
(82) Foster, M. D.; Rivin, I.; Treacy, M. M. J.; Delgado Friedrichs, O. *Microporous Mesoporous Mater.* **2006**, *90*, 32.
(83) Weisz, P. B.; Miale, J. N. *J. Catal.* **1965**, *4*, 527.
(84) Miale, J. N.; Chen, N. Y.; Weisz, P. B. *J. Catal.* **1966**, *6*, 278.
(85) Luzgin, M. V.; Stepanov, A. G.; Arzumanov, S. S.; Rogov, V. A.; Parmon, V. N.; Wang, W.; Hunger, M.; Freude, D. *Chem.—Eur. J.* **2006**, *12*, 457.
(86) De Moor, B. A.; Ghysels, A.; Reyniers, M. F.; van Speybroeck, V.; Waroquier, M.; Marin, G. B. *J. Chem. Theory Comput.* **2011**, *7*, 1090.
(87) Wielers, A. F. H.; Vaarkamp, M.; Post, M. F. M. *J. Catal.* **1991**, *127*, 51.